IEEE Access
Multidisciplinary | Rapid Review | Open Access Journal

Received May 4, 2019, accepted May 17, 2019, date of publication May 29, 2019, date of current version July 25, 2019.

Digital Object Identifier 10.1109/ACCESS.2019.2919749

Virtual Decomposition Based Modeling for Multi-DOF Manipulator With Flexible Joint

KERUI XIA[1,2,3], HONGJUN XING[2], LIANG DING[2], (Senior Member, IEEE), HAIBO GAO[2], GUANGJUN LIU[4], (Senior Member, IEEE), AND ZONGQUAN DENG[2]

[1]Department of Electrical Engineering, Tsinghua University, Beijing 100089, China
[2]State Key Laboratory of Robotics and System, Harbin Institute of Technology, Harbin 150001, China
[3]HRG International Institute for Research & Innovation, Hefei 230000, China
[4]Department of Aerospace Engineering, Ryerson University, Toronto, ON M5B 2K3, Canada

Corresponding authors: Hongjun Xing (xinghj@hit.edu.cn) and Liang Ding (liangding@hit.edu.cn)

This work was supported in part by the National Natural Science Foundation of China under Grant 51822502, in part by the Foundation for Innovative Research Groups of the Natural Science Foundation of China under Grant 51521003, in part by the Fundamental Research Funds for the Central Universities under Grant HIT.BRETIV.201903, and in part by the ''111 Project'' under Grant B07018.

ABSTRACT This paper discusses a problem that has plagued researchers for a long time regarding the dynamic modeling of a multiple degree-of-freedom (multi-DOF) manipulator such that its manipulation exhibits a higher computational efficiency and accuracy. Unknown friction, unknown gravitational torque, an uncertain moment of inertia, and severe joint coupling are the primary disturbing factors in multi-DOF manipulator modeling. In addition, joint flexible problems caused by the integration of harmonic drives increase the modeling complexity. Hitherto, no effective method has been found to address these problems. The virtual decomposition (VD)-based method exhibits the advantages of joint dynamics decoupling and minor computation compared with the traditional Lagrangian formulation or Newton–Euler formulation. In this study, an estimation method for the deformation-related torque of harmonic drives is established based on a novel experimental model; subsequently, this method is utilized in the VD-based model for the multi-DOF manipulator. Hence, the decoupling dynamic model for the manipulator considering joint flexibility is established. The performance of this new method has been evaluated by a contrast simulation with the Newton–Euler formulation, and the multi-DOF manipulator control simulation and experiment have been conducted with a VD-based model as a feedforward compensator to verify its performance in real-time control. The results demonstrated the validity and efficiency of e proposed approach.

INDEX TERMS Virtual decomposition, multi-DOF manipulator, dynamic modeling, joint flexibility.

I. INTRODUCTION

To realize safe and effective contact tasks using a multiple degree-of-freedom (multi-DOF) manipulator, the manipulator should demonstrate compliant motion capability to avoid undesired contact between it and objects [1]. A precise system dynamic model is essential for controlling the manipulator with compliant performance. When the number of joints is less than six, traditional methods such as the Lagrangian formulation [2], [3] and Newton–Euler formulation [4] can be used to establish the dynamic model of the manipulator. However, to improve the dexterity and enlarge the workspace of the manipulator, the latter is typically equipped with six or more joints; additionally, the joints are typically flexible because they are embedded with harmonic drives owing to their attractive properties such as high reduction ratio, compact size, lightweightness, and coaxial assembly. Owing to these characteristics of modern manipulators, traditional methods are incapable of modeling them precisely.

Using flexible joints renders the manipulator modeling even more complex, and many scholars have performed numerous studies regarding this. In 1987, Spong [5] established a dynamic model of a flexible joint. The joint was regarded as a linear spring with stiffness factor K, and the motor rotor was regarded as a whole body situated on a rotation shaft. With the two assumptions above, he utilized a four-order dynamic model to describe a flexible-joint robot. Khorasani [6] considered the effects of damping and reducer

The associate editor coordinating the review of this manuscript and approving it for publication was Chaoyong Li.

harmonic of a flexible joint and proposed a single link rigid-flexible coupling model based on the simplified flexible joint model proposed by Spong. In 1995, Bridges and Dawson [7] presented a more accurate flexible joint robot model that included the nonlinear factors of elasticity and friction. Ailon *et al*. [8] considered motor dynamics and parameter uncertainties to improve the previous dynamic model. A recursive decentralized control scheme was presented by Su *et al*. [9] to address the trajectory tracking problems of flexible manipulators, and the interconnections between the adjacent flexible links were calculated by recursive kinematics and dynamics. This scheme could achieve both trajectory tracking and vibration suppression for the flexible manipulator. Chaoui *et al*. [10] performed research on a flexible-joint robot with load uncertainty and discussed its modelling and control problems. Feedback linearization and sliding mode control have been used by Ramírez-Neria *et al*. [11] to improve the robust trajectory performance of a flexible-joint manipulator when unmodeled dynamics occur.

The dynamic models for flexible joints above are primarily based on the Lagrangian formulation, and the corresponding control methods present inherent defects in computation [12], [13]. Zhu [14] reported that the computation of the control algorithm based on the Lagrangian high-order dynamic model was proportional to the fourth power of the degree-of-freedom (DOF) of the robot. With the increase in the DOF, the complexity of the dynamic model and the computation cost will increase even faster; this problem severely limits the instantaneity of these algorithms and reduces the feasibility of the control system.

Hence, Zhu [14] proposed a novel theory based on virtual decomposition control (VDC) to solve the modeling and control problems of a multi-DOF robotic system. The primary concept of this method is to regard each joint or link of the manipulator as an independent subsystem. Each subsystem is connected with the contiguous subsystem through the ''force'' element composed of force and torque and the ''velocity'' element composed of the linear velocity and angular velocity, and the dynamic interactions between the subsystems is described using the virtual power flow. Compared with the dynamic model based on the Lagrangian formulation, the computation of this method is proportional only to the number of subsystems (DOFs); therefore, the computational efficiency is improved significantly. However, as a novel method to realize the dynamic modeling of a multi-DOF manipulator, the research on virtual decomposition (VD) is relatively scarce. In [15], Zhu and Schutter provided a new method to realize hybrid force/position control based on the VDC theory. Zhu *et al*. [16], [17] and Koivumäki and Mattila [18] introduced VDC into the control systems of modular robots, flexible-joint-based robots, and hydraulic-driving robots. Huang *et al*. [19] achieved adaptive impedance control and collision detection based on a VDC-based dynamic model and control theory; simulation and experimental results have proven the effectiveness of this method.

The VD-based dynamic modeling method uses the dynamics of subsystems to conduct the dynamic modeling of the entire robotic system, thereby the computational complexity of the system decreases significantly, only proportional to the number of subsystems; and the other advantage of employing the VD-based approach is that the alteration of one subsystem only affects the respective subsystem model equations, while keeping the model equations of the rest of the system unchanged.

The VD-based dynamic modeling method can be applied to robotic control; however, the effect of joint friction and flexibility caused by the reducer in the robot joint has rarely been addressed.

The primary contributions of this study are as follows: 1) A kinematic and dynamic model for a multi-DOF manipulator based on the VD-based modeling method is established. 2) The effect of friction and joint flexibility in the robot joint has been considered, the corresponding model has been established, and the entire decoupling dynamic model for the manipulator has been completed. 3) Simulation and experiment have been conducted to verify the effectiveness of the proposed modeling method in terms of accuracy and real-time capability.

The remainder of this paper is organized as follows: In Section II, the characteristics of flexible joints of a multi-DOF manipulator have been analyzed, and a VD-based dynamic model for them has been established. In Section III, the VD-based kinematic model and dynamic model for a six-DOF manipulator are described. A contrast simulation with the Newton–Euler formulation, and control simulation and experiment of a multi-DOF manipulator that demonstrate the validity and performance of the proposed method are presented in Section IV. Finally, conclusions are presented in Section V.

II. ANALYSIS AND VD-BASED MODELING FOR A HARMONIC DRIVE-BASED JOINT

Adequate torque output is a prerequisite for a manipulator to execute robotic operation, and the manipulator joint is typically integrated with a high load/mass ratio reducer to achieve impressive torque output capability. The high load/mass ratio reducers include a RV reducer with small flexibility and a harmonic drive with large flexibility. The introduction of these reducers renders the manipulator joint flexible, as shown in Fig. 1. This must be considered in designing the controller to eliminate the chattering effect caused by joint flexibility. Kiang *et al*. [20] and Rahimi *et al*. [21] reviewed the shortcomings of joint flexibility in terms of accurate position control, and the existing research findings were primarily based on a simplified dynamic model of the manipulator to design the control system. Regarding a multi-DOF manipulator with flexibility in a real scenario, these controllers typically do not demonstrate satisfactory performance.

This study focuses on decomposing a real manipulator into several subsystems virtually, including link subsystems and flexible joint subsystems; this technique is superior to the

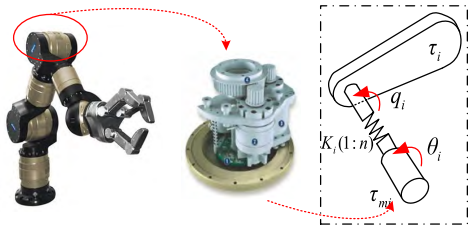

FIGURE 1. Joint flexibility caused by a reducer with high load/mass ratio.

traditional Newton-Euler formulation and Lagrangian formulation in terms of accuracy and efficiency.

A. DEFORMATION-RELATED TORQUE ESTIMATION METHOD FOR HARMONIC DRIVE

The structure of a conventional manipulator joint can be divided into four parts: joint base, motor rotor, reducer, and output link. The reducer is the primary factor of joint flexibility, and the reducer in this research is a harmonic drive (Harmonic Drive LLC 2012); the schematic illustration of the test joint is shown in Fig. 2. The position relationship among the wave generator, flexspline, and circular spline in the harmonic drive can be expressed as [22]

$$\theta_w = (\ell + 1)\theta_c - \ell\theta_f, \tag{1}$$

where ℓ is the reduction ratio; and θ_w, θ_c, and θ_f are the positions of the wave generator, circular spline, and flexspline, respectively.

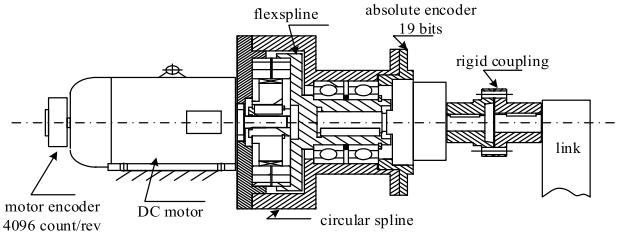

FIGURE 2. Schematic diagram of the test joint.

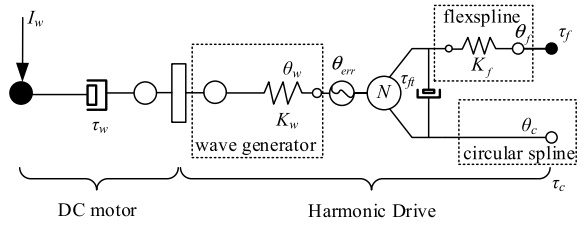

FIGURE 3. Schematic illustration of the test joint showing harmonic drive compliance components.

Fig. 3 illustrates the compliance behavior of the harmonic drives when the flexspline and wave generator compliance are considered. In Fig. 3, τ_f denotes the flexspline torque at the load side, τ_w denotes the torque of the wave generator center part, and τ_c denotes the circular spline torque. The angles θ_w and θ_c are measured by the link-side encoder and the motor-side encoder, respectively. K_w and K_f denote the local elastic coefficient for the wave generator and flexspline, respectively. τ_{ft} is the harmonic drive lumped friction torque.

The flexspline in the harmonic drive is a naturally deformable device; therefore, torsional deformations are demonstrated when a joint torque is applied. To describe this deformation-related torque, the following torque estimate is utilized; additional information regarding this method can be found in our previous work [23].

$$\tau_f = \frac{\tan(\Delta\theta_f c_f K_{f0})}{c_f}, \tag{2}$$

with

$$\Delta\theta_f = \Delta\theta - \frac{\mathrm{sgn}(\tau_w)}{c_w \ell K_{w0}}(1 - e^{-c_w|\tau_w|}) - \theta_{err}, \tag{3}$$

where $\Delta\theta$ is the total torsional deformation; θ_{err} is the kinematic error; K_{w0}, K_{f0}, c_w, and c_f are constants determined experimentally.

B. VD-BASED KINEMATICS AND DYNAMICS FOR HARMONIC-DRIVE-BASED JOINT

According to the conclusions regarding flexible joints in Section II.A, deformation-related torques exist between the motor output and link output. Additionally, friction and other factors will cause disturbances in completing the entire manipulator modeling; thus, we should further conduct a virtual decomposition to the flexible joint by setting two cutting points that are in the joint base and joint output link. The motor stator of the joint is fixed with the joint base as part of the base, and the motor rotor is connected with the joint output link through the harmonic drive.

The flexible joint structure diagram based on virtual decomposition is shown in Fig. 4, in which $\{\mathbf{T}\}$ is the coordinate system fixed on the output link, $\{\mathbf{D}\}$ is the coordinate system fixed on the motor rotor, and $\{\mathbf{B}\}$ is the coordinate system fixed on the joint base.

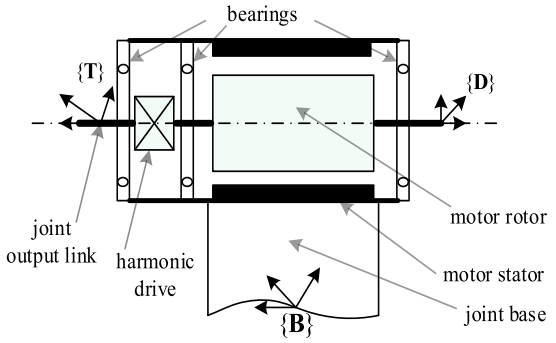

FIGURE 4. Flexible joint structure diagram based on virtual decomposition.

The harmonic drive can be divided into two parts: one part is connected with the joint output link, and the other is connected with the motor rotor. The entire joint can be viewed

as three parts: joint base, motor rotor, and joint output link. We define $\ell \geq 1$ as the reduction ratio of the harmonic drive, q as the joint position, and $\ell\kappa$ as the motor rotor position. Subsequently, the velocity relationship between the motor rotor and joint output link can be expressed as

$$^{\mathbf{D}}\boldsymbol{V} = z_\tau \ell \dot{\boldsymbol{\kappa}} + {}^{\mathbf{B}}\boldsymbol{U}_{\mathbf{D}}^{\mathrm{T}\,\mathbf{B}}\boldsymbol{V}, \tag{4}$$

$$^{\mathbf{T}}\boldsymbol{V} = z_\tau \dot{\boldsymbol{q}} + {}^{\mathbf{B}}\boldsymbol{U}_{\mathbf{T}}^{\mathrm{T}\,\mathbf{B}}\boldsymbol{V}, \tag{5}$$

where $z_\tau = [0, 0, 0, 0, 0, 1]^{\mathrm{T}} \in \mathbb{R}^6$, and $\boldsymbol{U}$ is a generalized force/torque transformation matrix that will be described in the next section.

The dynamics of the joint base, motor rotor, and joint output link can be expressed as

$$^{\mathbf{B}}\boldsymbol{F}^* = \boldsymbol{M}_{\mathbf{B}}\,{}^{\mathbf{B}}\dot{\boldsymbol{V}} + \boldsymbol{C}_{\mathbf{B}}({}^{\mathbf{B}}\boldsymbol{\omega})\,{}^{\mathbf{B}}\boldsymbol{V} + \boldsymbol{G}_{\mathbf{B}}, \tag{6}$$

$$^{\mathbf{D}}\boldsymbol{F}^* = \boldsymbol{M}_{\mathbf{D}}\,{}^{\mathbf{D}}\dot{\boldsymbol{V}} + \boldsymbol{C}_{\mathbf{D}}({}^{\mathbf{D}}\boldsymbol{\omega})\,{}^{\mathbf{D}}\boldsymbol{V} + \boldsymbol{G}_{\mathbf{D}}, \tag{7}$$

$$^{\mathbf{T}}\boldsymbol{F}^* = \boldsymbol{M}_{\mathbf{T}}\,{}^{\mathbf{T}}\dot{\boldsymbol{V}} + \boldsymbol{C}_{\mathbf{T}}({}^{\mathbf{T}}\boldsymbol{\omega})\,{}^{\mathbf{T}}\boldsymbol{V} + \boldsymbol{G}_{\mathbf{T}}, \tag{8}$$

respectively, where the detailed expressions of $\boldsymbol{M}_{\mathrm{B}}, \boldsymbol{C}_{\mathrm{B}}, \boldsymbol{G}_{\mathrm{B}}$, $\boldsymbol{M}_{\mathrm{D}}, \boldsymbol{C}_{\mathrm{D}}, \boldsymbol{G}_{\mathrm{D}}, \boldsymbol{M}_{\mathrm{T}}, \boldsymbol{C}_{\mathrm{T}},$ and $\boldsymbol{G}_{\mathrm{T}}$ are shown in **Appendix** with the appropriate frame substitutions.

We define the following symbols: $^{\mathbf{T}}\boldsymbol{F}_{\mathrm{q}} \in \mathbb{R}^6$ represents the force/torque vector from the joint base to the joint output link expressed in $\{\mathbf{T}\}$; $^{\mathbf{D}}\boldsymbol{F}_{\kappa} \in \mathbb{R}^6$ represents the force/torque vector from the joint base to the motor rotor expressed in $\{\mathbf{D}\}$; $^{\mathbf{T}}\boldsymbol{F} \in \mathbb{R}^6$ represents the force/torque vector from the motor output to the adjacent link expressed in $\{\mathbf{T}\}$, which acts on the driving cutting point; $^{\mathbf{F}}\boldsymbol{F} \in \mathbb{R}^6$ represents the force/torque vector from the adjacent link to the joint output link expressed in $\{\mathbf{F}\}$, which acts on the driven cutting point. $-\xi(q, \dot{q}) \in \mathbb{R}$ is a friction torque applied to the joint output link from the joint base; $-\xi(\kappa, \dot{\kappa}) \in \mathbb{R}$ is a friction torque applied to the motor rotor from the joint base; $\tau_t \in \mathbb{R}$ is the effective input torque of the drive; $\tau \in \mathbb{R}$ is the motor control torque except the deformation-related torque defined in (2) and (3).

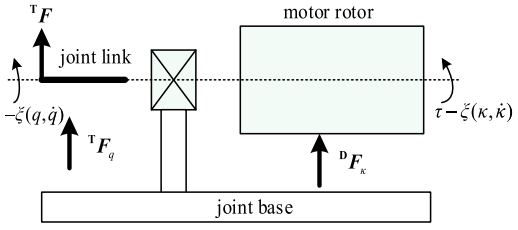

FIGURE 5. Internal force diagram of a flexible joint.

Fig. 5 shows the internal force diagram of the flexible joint. Combined with the definition of the force symbols, we can obtain

$$^{\mathbf{T}}\boldsymbol{F}^* = -{}^{\mathbf{T}}\boldsymbol{F} + {}^{\mathbf{T}}\boldsymbol{F}_q, \tag{9}$$

$$^{\mathbf{D}}\boldsymbol{F}^* = {}^{\mathbf{D}}\boldsymbol{F}_\kappa, \tag{10}$$

$$^{\mathbf{B}}\boldsymbol{F}^* = {}^{\mathbf{B}}\boldsymbol{F} - {}^{\mathbf{B}}\boldsymbol{U}_T\,{}^{\mathbf{T}}\boldsymbol{F}_q - {}^{\mathbf{B}}\boldsymbol{U}_D\,{}^{\mathbf{D}}\boldsymbol{F}_\kappa, \tag{11}$$

where $z_\tau^{\mathrm{T}}{}^{\mathbf{T}}\boldsymbol{F}_q = \ell\tau_t - \xi(q, \dot{q}), z_\tau^{\mathrm{T}}{}^{\mathbf{D}}\boldsymbol{F}_\kappa = \tau - \tau_t - \xi(\kappa, \dot{\kappa})$.

C. FEEDFORWARD MODEL FOR HARMONIC DRIVE-BASED JOINT

The feedforward model for the harmonic drive-based joint comprises three steps, as will be described as follows:

1) REQUIRED VELOCITIES

The terminology of "required velocity" is an important concept in the VD approach. A required velocity is different from a desired velocity that typically serves as the reference trajectory of a velocity with respect to time. In the joint space, the required joint velocities are designed as

$$\dot{\boldsymbol{q}}_r = \dot{\boldsymbol{q}}_d + \boldsymbol{\Lambda}(\boldsymbol{q}_d - \boldsymbol{q}) \tag{12}$$

to realize the exponential convergence of the system, where $\dot{\boldsymbol{q}}_d$ is the desired joint velocity vector, and $\boldsymbol{\Lambda} \in \mathbb{R}^{n\times n}$ is a diagonal positive definite symmetric matrix. It is noteworthy that the required velocities in each body system can be calculated based on the required joint velocities and coordinate transformation shown in (4) and (5).

The required linear velocities and angular velocities of the flexible joint after virtual decomposition can be expressed as

$$^{\mathbf{D}}\boldsymbol{V}_r = z_\tau \ell \dot{\boldsymbol{\kappa}}_r + {}^{\mathbf{B}}\boldsymbol{U}_{\mathbf{D}}^{\mathrm{T}\,\mathbf{B}}\boldsymbol{V}_r, \tag{13}$$

$$^{\mathbf{T}}\boldsymbol{V}_r = z_\tau \dot{\boldsymbol{q}}_r + {}^{\mathbf{B}}\boldsymbol{U}_{\mathbf{T}}^{\mathrm{T}\,\mathbf{B}}\boldsymbol{V}_r, \tag{14}$$

where $\dot{\boldsymbol{q}}_r$ and $\dot{\boldsymbol{\kappa}}_r$ represent the required joint velocities and motor rotor velocities, respectively.

2) REQUIRED NET FORCE/TORQUE VECTORS

The required net force/torque vectors on joint base, motor rotor and joint output link can be calculated as follows

$$^{\mathbf{T}}\boldsymbol{F}_r^* = {}^{\mathbf{T}}\boldsymbol{F}^* + \boldsymbol{K}_{\mathbf{T}}({}^{\mathbf{T}}\boldsymbol{V}_r - {}^{\mathbf{T}}\boldsymbol{V}), \tag{15}$$

$$^{\mathbf{D}}\boldsymbol{F}_r^* = {}^{\mathbf{D}}\boldsymbol{F}^* + \boldsymbol{K}_{\mathbf{D}}({}^{\mathbf{D}}\boldsymbol{V}_r - {}^{\mathbf{D}}\boldsymbol{V}), \tag{16}$$

$$^{\mathbf{B}}\boldsymbol{F}_r^* = {}^{\mathbf{B}}\boldsymbol{F}^* + \boldsymbol{K}_{\mathbf{B}}({}^{\mathbf{B}}\boldsymbol{V}_r - {}^{\mathbf{B}}\boldsymbol{V}), \tag{17}$$

where $\boldsymbol{K}_{\mathbf{B}} \in \mathbb{R}^{6\times6}$, $\boldsymbol{K}_{\mathbf{D}} \in \mathbb{R}^{6\times6}$ and $\boldsymbol{K}_{\mathbf{T}} \in \mathbb{R}^{6\times6}$ are all positive definite gain matrices.

3) REQUIRED FORCE/TORQUE VECTOR TRANSFORMATIONS

The force/torque vectors on the joint base, motor rotor, and joint output link by constraints can be expressed as

$$^{\mathbf{T}}\boldsymbol{F}_r^* = -{}^{\mathbf{T}}\boldsymbol{F}_r + {}^{\mathbf{T}}\boldsymbol{F}_{qr}, \tag{18}$$

$$^{\mathbf{D}}\boldsymbol{F}_r^* = {}^{\mathbf{D}}\boldsymbol{F}_{\kappa r}, \tag{19}$$

$$^{\mathbf{B}}\boldsymbol{F}_r^* = {}^{\mathbf{B}}\boldsymbol{F}_r - {}^{\mathbf{B}}\boldsymbol{U}_T\,{}^{\mathbf{T}}\boldsymbol{F}_{qr} - {}^{\mathbf{B}}\boldsymbol{U}_D\,{}^{\mathbf{D}}\boldsymbol{F}_{\kappa r}. \tag{20}$$

The force/torque vectors above can be further expressed as

$$z_\tau^{T}{}^{\mathbf{T}}\boldsymbol{F}_{qr} = \ell\left[\tau_t - k_{vq}(\dot{q}_{\mathrm{r}} - \dot{q})\right] - \xi(q, \dot{q}), \tag{21}$$

$$z_\tau^{\mathrm{T}\mathbf{D}}\boldsymbol{F}_{\kappa r} = \tau - \tau_t - k_{v\kappa}(\dot{\kappa}_r - \dot{\kappa}) - \xi(\kappa, \dot{\kappa}), \tag{22}$$

where $k_{vq} > 0$ and $k_{v\kappa} > 0$ are two gain matrices.

According to (18)–(22), the harmonic-drive-based joint control law can be rewritten as follows:

$$^{\mathbf{T}}\boldsymbol{F}_{qr} = {}^{\mathbf{T}}\boldsymbol{F}_r^* + {}^{\mathbf{T}}\boldsymbol{F}_r, \tag{23}$$

$$^{\mathbf{D}}\boldsymbol{F}_{\kappa r} = {}^{\mathbf{D}}\boldsymbol{F}_r^*, \tag{24}$$

$$^{\mathbf{B}}\boldsymbol{F}_r = {}^{\mathbf{B}}\boldsymbol{F}_r^* + {}^{\mathbf{B}}\boldsymbol{U}_T{}^{\mathbf{T}}\boldsymbol{F}_{qr} + {}^{\mathbf{B}}\boldsymbol{U}_D{}^{\mathbf{D}}\boldsymbol{F}_{\kappa r}, \tag{25}$$

$$\tau_t = \frac{1}{\ell}\left(z_\tau^T{}^{\mathbf{T}}\boldsymbol{F}_{qr} + \xi(q,\dot{q})\right) + k_{vq}(\dot{q}_r - \dot{q}), \tag{26}$$

$$\tau = \tau_t + k_{v\kappa}(\dot{\kappa}_r - \dot{\kappa}) + \xi(\kappa,\dot{\kappa}) + z_\tau^{\mathbf{TD}}\boldsymbol{F}_{\kappa r}. \tag{27}$$

Thus, with the deformation-related torque τ_f defined in (2) and (3), the entire motor control torque τ_m is

$$\tau_m = \tau + \tau_f. \tag{28}$$

III. VD-BASED MODEL FOR MULTI-DOF MANIPULATOR

The research on VD-based models for flexible joints with friction and other factors can be conducted according to the results of Sections I and II. A VD-based link model still needs to be constructed to complete the entire dynamic model for a multi-DOF manipulator. The six-DOF manipulator is virtually decomposed into 12 subsystems, with each containing a single link or a single joint, by placing 11 cutting points into the system. The force/torque transformations between these subsystems are provided.

A. DESCRIPTION OF THE 6-DOF MANIPULATOR

The description of the six-DOF manipulator is shown in Fig. 6; it has six revolute joints and six links, additional information regarding this manipulator can be found in [23]. And it should be noted that the VD-based modeling method is not limited to revolute joints, it is also applicable to prismatic joints and spherical joints. The distance between joint1 and joint2 is l_1, the rotation axes among joint2, joint3, and joint5 are parallel, and the distances among these axes are l_2 and l_3 in sequence. Additionally, l_4 represents the distance between joint5 and the end-effector. The coordinate systems of the manipulator are shown in the right subfigure of Fig. 6. To establish the VD-based model for the manipulator, we virtually decomposed it into six revolute joints and six links. Frame $\{\mathbf{B}_i\}$, $i = 1,\ldots,6$, is fixed with the i^{th} joint and its z axis coincides with the rotation axis of the joint; frame $\{\mathbf{T}_i\}$, $i = 2,\ldots,6$, is fixed with the end of the $(i\text{-}1)^{\text{th}}$ link and its z axis coincides with the rotation axis of the i^{th} joint; and $\{\mathbf{I}\}$ is the world frame.

B. VD-BASED KINEMATICS AND DYNAMICS FOR THE MANIPULATOR

The manipulator in Fig. 6 is composed of six joints. The relationship of the joint angular velocities in the joint space is

$$^{\mathbf{B}_1}\boldsymbol{V} = z\dot{q}_1, \tag{29}$$

$$^{\mathbf{T}_i}\boldsymbol{V} = {}^{\mathbf{B}_{i-1}}\boldsymbol{U}_{\mathbf{T}_i}^{\mathbf{T}}{}^{\mathbf{B}_{i-1}}\boldsymbol{V}, \tag{30}$$

$$^{\mathbf{B}_i}\boldsymbol{V} = z\dot{q}_i + {}^{\mathbf{T}_i}\boldsymbol{U}_{\mathbf{B}_i}^{\mathbf{T}}{}^{\mathbf{T}_i}\boldsymbol{V} = z\dot{q}_i + {}^{\mathbf{B}_{i-1}}\boldsymbol{U}_{\mathbf{B}_i}^{\mathbf{T}}{}^{\mathbf{B}_{i-1}}\boldsymbol{V}, \tag{31}$$

where $i = 2,3,4,5$, $z = [0,0,0,0,0,1]^{\mathrm{T}} \in \mathbb{R}^6$, $\dot{q}_i$ represents the angular velocity of the i^{th} joint, and $^{\mathbf{T}}\boldsymbol{U}_{\mathbf{B}}$ is the generalized force/torque transformation matrix from $\{\mathbf{B}\}$ to $\{\mathbf{T}\}$ of the following form:

$$^{\mathbf{T}}\boldsymbol{U}_{\mathbf{B}} = \begin{bmatrix} {}^{\mathbf{T}}\boldsymbol{R}_{\mathbf{B}} & \boldsymbol{0} \\ ({}^{\mathbf{T}}\boldsymbol{P}_{\mathbf{B}}\times){}^{\mathbf{T}}\boldsymbol{R}_{\mathbf{B}} & {}^{\mathbf{T}}\boldsymbol{R}_{\mathbf{B}} \end{bmatrix} \in \mathbb{R}^{6\times 6}, \tag{32}$$

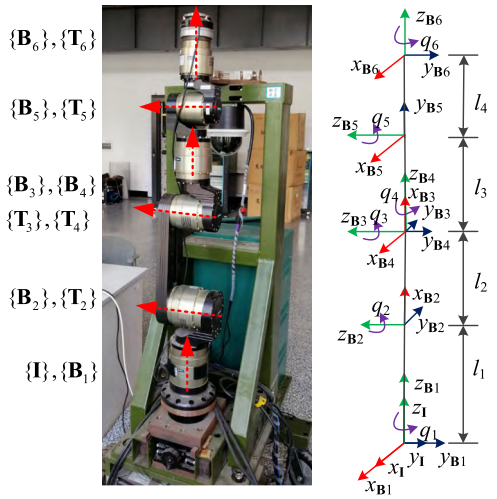

FIGURE 6. Description of the 6-DOF manipulator.

where $^{\mathbf{T}}\boldsymbol{R}_{\mathbf{B}}$ and $^{\mathbf{T}}\boldsymbol{P}_{\mathbf{B}}$ are the rotation transformation matrix and translation transformation matrix from $\{\mathbf{B}\}$ to $\{\mathbf{T}\}$, respectively.

The generalized coordinate transformation matrix of the manipulator is defined as

$$^{T}\mathrm{T}_{B} = \begin{bmatrix} {}^{T}\mathrm{R}_{\mathbf{B}} & {}^{T}\mathrm{P}_{\mathbf{B}} \\ 0 & 1 \end{bmatrix}, \tag{33}$$

and according to Fig. 6, the transformation matrices for the manipulator can be obtained as

$$^{I}\mathrm{T}_{\mathbf{B}_1} = \begin{bmatrix} c_1 & -s_1 & 0 & 0 \\ s_1 & c_1 & 0 & 0 \\ 0 & 0 & 1 & 0 \\ 0 & 0 & 0 & 1 \end{bmatrix}, \; ^{T_2}\mathrm{T}_{\mathbf{B}_2} = \begin{bmatrix} c_2 & -s_2 & 0 & 0 \\ 0 & 0 & -1 & 0 \\ s_2 & c_2 & 0 & 0 \\ 0 & 0 & 0 & 1 \end{bmatrix}, \tag{34}$$

$$^{T_3}\mathrm{T}_{\mathbf{B}_3} = \begin{bmatrix} c_3 & -s_3 & 0 & 0 \\ s_3 & c_3 & 0 & 0 \\ 0 & 0 & 1 & 0 \\ 0 & 0 & 0 & 1 \end{bmatrix}, \; ^{T_4}\mathrm{T}_{\mathbf{B}_4} = \begin{bmatrix} 0 & 0 & 1 & 0 \\ -c_4 & s_4 & 0 & 0 \\ -s_4 & -c_4 & 0 & 0 \\ 0 & 0 & 0 & 1 \end{bmatrix}, \tag{35}$$

$$^{T_5}\mathrm{T}_{\mathbf{B}_5} = \begin{bmatrix} c_5 & -s_5 & 0 & 0 \\ 0 & 0 & -1 & 0 \\ s_5 & c_5 & 0 & 0 \\ 0 & 0 & 0 & 1 \end{bmatrix}, \; ^{T_6}\mathrm{T}_{\mathbf{B}_6} = \begin{bmatrix} c_6 & -s_6 & 0 & 0 \\ 0 & 0 & 1 & 0 \\ -s_6 & -c_6 & 0 & 0 \\ 0 & 0 & 0 & 1 \end{bmatrix}, \tag{36}$$

where $s_i = \sin(q_i)$, $c_i = \cos(q_i)$, $i = 1,\ldots,6$.

The transformation matrices from $\{\mathbf{T}_i\}$ to $\{\mathbf{B}_{i-1}\}$, $i = 2,\ldots,6$, denoted as $^{\mathbf{B}_1}\boldsymbol{T}_{\mathbf{T}_2}$, $^{\mathbf{B}_2}\boldsymbol{T}_{\mathbf{T}_3}$, $^{\mathbf{B}_3}\boldsymbol{T}_{\mathbf{T}_4}$, $^{\mathbf{B}_4}\boldsymbol{T}_{\mathbf{T}_5}$, $^{\mathbf{B}_5}\boldsymbol{T}_{\mathbf{T}_6}$, can be obtained easily because these matrices are all translation transformation matrices.

The first step in establishing the kinematic model for the manipulator based on the VD approach is to build the velocity mapping matrix from the Cartesian space to joint space, that is, the Jacobian matrix in the Lagrangian formulation or Newton–Euler formulation. Many methods can be used to

obtain the Jacobian matrix of a manipulator. In this study, we obtain it by the vector product method.

We define the frame associated with the end-effector as $\{\mathbf{O}\}$, and the Cartesian velocity is denoted as $V = {}^{O}\boldsymbol{V}$. The relationship between ${}^{O}\boldsymbol{V}$ and the joint velocity $\dot{\boldsymbol{q}} = [\dot{q}_1, \cdots, \dot{q}_6] \in \mathbb{R}^6$ is controlled by Jacobian matrix $\boldsymbol{J}_q$ as follows:

$$ {}^{\mathbf{O}}\boldsymbol{V} = \boldsymbol{J}_q \dot{\boldsymbol{q}}, \tag{37} $$

with

$$ \boldsymbol{J}_q = \begin{bmatrix} {}^{\mathbf{B_1}}\mathbf{U}_{\mathbf{O}}^{\mathrm{T}}\mathbf{z} & {}^{\mathbf{B_2}}\mathbf{U}_{\mathbf{O}}^{\mathrm{T}}\mathbf{z} & {}^{\mathbf{B_3}}\mathbf{U}_{\mathbf{O}}^{\mathrm{T}}\mathbf{z} \\ & {}^{\mathbf{B_4}}\mathbf{U}_{\mathbf{O}}^{\mathrm{T}}\mathbf{z} \quad {}^{\mathbf{B_5}}\mathbf{U}_{\mathbf{O}}^{\mathrm{T}}\mathbf{z} \quad {}^{\mathbf{B_6}}\mathbf{U}_{\mathbf{O}}^{\mathrm{T}}\mathbf{z} \end{bmatrix}^{\mathrm{T}} \in \mathbb{R}^{6\times 6}. \tag{38} $$

The relationship between joint space velocity and workspace velocity can be expressed as

$$ \mathcal{V}_a = \mathcal{J}_a \mathcal{V}, \tag{39} $$

where $\mathcal{J}_a = \boldsymbol{J}_q^{-1}$, and $\mathcal{V}_a = \dot{\boldsymbol{q}} \in \mathbb{R}^6$ is the joint space velocity.

The next step is to build the mapping matrix from the joint space velocity $\mathcal{V}_a$ to the generalized velocity $\mathcal{V}_b$. The generalized velocity $\mathcal{V}_b$ consists of all the linear velocities and angular velocities, which is expressed as

$$ \mathcal{V}_b = \left[{}^{\mathrm{O}}\boldsymbol{V}^{\mathbf{T}}, {}^{\mathbf{B_1}}\boldsymbol{V}^{\mathbf{T}}, \cdots, {}^{\mathbf{B}_k}\boldsymbol{V}^{\mathbf{T}}, \cdots, {}^{\mathbf{B_6}}\boldsymbol{V}^{\mathbf{T}} \right]^{\mathbf{T}} \in \mathbb{R}^{42}. \tag{40} $$

The relationship among $\mathcal{V}$, $\mathcal{V}_b$, and $\mathcal{V}_a$ is expressed as

$$ \mathcal{V}_b = \mathcal{J}_b \mathcal{V} = \mathcal{J}_{ba} \mathcal{J}_a \mathcal{V} = \mathcal{J}_{ba} \mathcal{V}_a, \tag{41} $$

where

$$ \mathcal{J}_{ba} = \begin{bmatrix} & \boldsymbol{J}_q & & \\ \begin{bmatrix} z & \mathbf{0} & \cdots & \mathbf{0} \\ {}^{\mathbf{B}_1}\boldsymbol{U}_{\mathbf{B}_2}^{\mathrm{T}} z & z & \cdots & \mathbf{0} \\ \vdots & \cdots & \ddots & \vdots \\ {}^{\mathbf{B}_1}\boldsymbol{U}_{\mathbf{B}_6}^{\mathrm{T}} \mathbf{z} & {}^{\mathbf{B}_2}\boldsymbol{U}_{\mathbf{B}_6}^{\mathrm{T}} z & \cdots & z \end{bmatrix} \end{bmatrix} \in \mathbb{R}^{72\times 6}, $$

and $\mathcal{J}_b = \mathcal{J}_{ba}\mathcal{J}_a$.

The entire generalized velocity vector $\mathcal{V}_e$ of the manipulator system is defined as

$$ \mathcal{V}_e = \left[{}^{\mathrm{O}}\boldsymbol{V}^{\mathbf{T}}, \dot{\boldsymbol{q}}^{\mathbf{T}}, {}^{\mathbf{B}_1}\boldsymbol{V}^{\mathbf{T}}, \cdots, {}^{\mathbf{B}_k}\boldsymbol{V}^{\mathbf{T}}, \cdots, {}^{\mathbf{B_6}}\boldsymbol{V}^{\mathbf{T}} \right]^{\mathbf{T}} \in \mathbb{R}^{48}, \tag{42} $$

and the mapping from $\mathcal{V}$ to $\mathcal{V}_e$ can be obtained as

$$ \mathcal{V}_e = \mathcal{J}_e \mathcal{V}, \tag{43} $$

where $\mathcal{J}_e \in \mathbb{R}^{48\times 6}$ is an extended Jacobian matrix.

The definitions above are highly important for building the forward dynamics of a multi-DOF manipulator, and is essential in establishing the control plant in robot simulations [24].

The force resultant equations for the six links can be calculated as

$$ {}^{\mathbf{B}_6}\boldsymbol{F}^* = {}^{\mathbf{B}_6}\boldsymbol{F} - \boldsymbol{F}_e, \tag{44} $$

$$ {}^{\mathbf{T}_i}\boldsymbol{F} = {}^{\mathbf{T}_i}\boldsymbol{U}_{\mathbf{B}_i} {}^{\mathbf{B}_i}\boldsymbol{F}, \quad i = 6, \cdots, 1, \tag{45} $$

$$ {}^{\mathbf{B}_i}\boldsymbol{F}^* = {}^{\mathbf{B}_i}\boldsymbol{F} - {}^{\mathbf{B}_i}\boldsymbol{U}_{\mathbf{T}_{i+1}} {}^{\mathbf{T}_{i+1}}\boldsymbol{F}, \quad i = 5, \cdots, 1, \tag{46} $$

where $\boldsymbol{F}_e$ is the external contact force exerted at the end of the manipulator, and ${}^{\mathbf{B}_i}\boldsymbol{F}^*$ is the independent link force for the i^{th} link with the following form:

$$ {}^{\mathbf{B}_i}\boldsymbol{F}^* = \boldsymbol{M}_{\mathbf{B}_i} {}^{\mathbf{B}_i}\dot{\boldsymbol{V}} + \boldsymbol{C}_{\mathbf{B}_i}({}^{\mathbf{B}_i}\boldsymbol{\omega}) {}^{\mathbf{B}_i}\boldsymbol{V} + \boldsymbol{G}_{\mathbf{B}_i}, \quad i = 1, \cdots, 6, \tag{47} $$

where the detailed expressions of $\boldsymbol{M}_{\mathbf{B}_i}$, $\boldsymbol{C}_{\mathbf{B}_i}$, $\boldsymbol{G}_{\mathbf{B}_i}$ are shown in **Appendix** with the appropriate frame substitutions, and ${}^{\mathbf{B}_i}\boldsymbol{V}$ is the velocity and angular velocity of each link expressed in its own system.

In (47), the angular velocities for the manipulator links can be obtained using (29) – (36), which are

$$ {}^{\mathbf{B}_1}\boldsymbol{\omega} = \begin{bmatrix} 0 \\ 0 \\ \dot{q}_1 \end{bmatrix}, \quad {}^{\mathbf{B}_2}\boldsymbol{\omega} = \begin{bmatrix} \dot{q}_1 s_2 \\ \dot{q}_1 c_2 \\ \dot{q}_2 \end{bmatrix}, \quad {}^{\mathbf{B}_3}\boldsymbol{\omega} = \begin{bmatrix} \dot{q}_1 s_{23} \\ \dot{q}_1 c_{23} \\ \vartheta_1 \end{bmatrix}, $$

$$ {}^{\mathbf{B}_4}\boldsymbol{\omega} = \begin{bmatrix} -\vartheta_1 s_4 - \dot{q}_1 c_{23} c_4 \\ \dot{q}_1 c_{23} s_4 - \vartheta_1 c_4 \\ \vartheta_2 \end{bmatrix}, $$

$$ {}^{\mathbf{B}_5}\boldsymbol{\omega} = \begin{bmatrix} \vartheta_2 s_5 - \vartheta_3 c_5 \\ \vartheta_2 c_5 - \vartheta_3 s_5 \\ \dot{q}_5 + \vartheta_1 c_4 - \dot{q}_1 c_{23} s_4 \end{bmatrix}, $$

$$ {}^{\mathbf{B}_6}\boldsymbol{\omega} = \begin{bmatrix} -(\vartheta_3 c_5 - \vartheta_2 s_5) c_6 - (\dot{q}_5 + \vartheta_1 c_4 - \dot{q}_1 c_{23} s_4) s_6 \\ (\vartheta_3 c_5 - \vartheta_2 s_5) s_6 - (\dot{q}_5 + \vartheta_1 c_4 - \dot{q}_1 c_{23} s_4) c_6 \\ \dot{q}_6 + \vartheta_3 s_5 + \vartheta_2 c_5 \end{bmatrix}, $$

where $s_i = \sin(q_i)$, $c_i = \cos(q_i)$, $s_{ij} = \sin(q_i + q_j)$, $c_{ij} = \cos(q_i + q_j)$, $i = 1, \ldots, 6, j = 1, \ldots, 6$, and $\vartheta_1 = \dot{q}_2 + \dot{q}_3$, $\vartheta_2 = \dot{q}_4 + \dot{q}_1 s_{23}$, $\vartheta_3 = (\dot{q}_2 + \dot{q}_3) s_4 + \dot{q}_1 c_{23} c_4$.

According to the generalized coordinate transformation matrices and (32), the force/torque transformation matrices between any two coordinate systems can be calculated.

C. FEEDFORWARD MODEL FOR THE MANIPULATOR

The manipulator described in Fig. 6 contains six joints. The desired and required joint position vectors are defined as $\boldsymbol{q}_d = \left[q_{1d}, \cdots, q_{6d} \right]^{\mathrm{T}} \in \mathbb{R}^6$ and $\dot{\boldsymbol{q}}_r = \dot{\boldsymbol{q}}_d + \boldsymbol{\Lambda}(\boldsymbol{q}_d - \boldsymbol{q})$, respectively, where $\boldsymbol{\Lambda} \in \mathbb{R}^{6\times 6}$ is a diagonal positive definite symmetric matrix.

1) REQUIRED VELOCITIES

The required linear velocities and angular velocities for the links in their body frames can be expressed as

$$ {}^{\mathbf{B}_1}\boldsymbol{V}_r = z \dot{q}_{1r}, \tag{48} $$

$$ {}^{\mathbf{B}_i}\boldsymbol{V}_r = z \dot{q}_{ir} + {}^{\mathbf{B}_{i-1}}\boldsymbol{U}_{\mathbf{B}_i}^{\mathrm{T}} {}^{\mathbf{B}_{i-1}}\boldsymbol{V}_r. \tag{49} $$

2) REQUIRED NET FORCE/TORQUE VECTORS

The required net force/torque vectors for the links can be calculated as follows:

$$ {}^{\mathbf{B}_i}\boldsymbol{F}_r^* = {}^{\mathbf{B}_i}\boldsymbol{F}^* + \boldsymbol{K}_{\mathbf{B}_i}({}^{\mathbf{B}_i}\boldsymbol{V}_r - {}^{\mathbf{B}_i}\boldsymbol{V}), \quad \boldsymbol{i} = 1, \cdots, 6, \tag{50} $$

where $\boldsymbol{K}_{\mathbf{B}_i} \in \mathbb{R}^{6\times 6}$ is a positive definite gain matrix.

3) REQUIRED FORCE/TORQUE VECTOR TRANSFORMATIONS

The force/torque vectors for the links by constraints can be expressed as

$$^{\mathbf{B}_6}\boldsymbol{F}_r = {}^{\mathbf{B}_6}\boldsymbol{F}_r^* + \boldsymbol{F}_e, \tag{51}$$

$$^{\mathbf{T}_i}\boldsymbol{F}_r = {}^{\mathbf{T}_i}\boldsymbol{U}_{\mathbf{B}_i}{}^{\mathbf{B}_i}\boldsymbol{F}_r, \quad i = 6, \cdots, 1, \tag{52}$$

$$^{\mathbf{B}_i}\boldsymbol{F}_r = {}^{\mathbf{B}_i}\boldsymbol{F}_r^* + {}^{\mathbf{B}_i}\boldsymbol{U}_{\mathbf{T}_{i+1}}{}^{\mathbf{T}_{i+1}}\boldsymbol{F}_r, \quad i = 5, \cdots, 1. \tag{53}$$

IV. SIMULATION AND EXPERIMENT

The VD-based modeling method uses the dynamics of the subsystems (rigid links and flexible joints) to build the entire dynamic model for the multi-DOF manipulator, thus improving the computational efficiency while maintaining accuracy. To illustrate the validity of the proposed method, simulations have been conducted.

A. CONTRAST SIMULATION WITH NEWTON–EULER FORMULATION

The Newton–Euler formulation is a widespread method for analyzing the dynamics of robotic manipulators [25]. In this section, we compare the results of the VD-based method with the Newton–Euler formulation to demonstrate the superiority of the proposed method in addressing the dynamics of a complex manipulator.

The plant we used in our simulation was a six-DOF manipulator, as shown in Fig. 6, equipped with a harmonic drive in each joint. The parameters of the manipulator are shown in Table 1. The lengths of the links of the manipulator were set as $l_1 = 0.3$ m, $l_2 = 0.3$ m, $l_3 = 0.303$ m, and $l_4 = 0.5$ m. The reduction ratio of the harmonic drive in the simulation was $\ell = 100$, and the parameters for deformation-related torque were obtained according to [26]. The friction torque applied to the joint output link from the joint base is defined as

$$\xi(q, \dot{q}) = \left[f_c + (f_s - f_c)e^{-|\dot{q}/v_s|^2}\right]\mathrm{sgn}(\dot{q}) + f_v\dot{q}, \tag{54}$$

where f_c, f_s, f_v are the Coulomb, static, and viscous friction coefficients, respectively. The parameter v_s is the Stribeck parameter. The friction torque applied to the motor rotor from the joint base is simplified as

$$\xi(\kappa, \dot{\kappa}) = f_{c\kappa}, \tag{55}$$

where $f_{c\kappa}$ is the Coulomb coefficient. The friction setting above is feasible because the link-side friction and motor-side friction can be interchanged; in practice, the joint friction is typically identified as one item, that is, the motor-side friction $\xi(\kappa, \dot{\kappa})$ is omitted. The simulation joint friction coefficients, as shown in Table 2, are generated primarily based on [27]. For simplification, the motion of the motor rotor is assumed to be a pure rotation along the joint axis, that is,

$$\boldsymbol{z}_\tau^{\mathbf{TD}}\boldsymbol{F}^* = I_m\ddot{\boldsymbol{\kappa}}, \tag{56}$$

where I_m represents the moment of inertia of the rotor multiplied by the reduction ratio ℓ, and we set $I_m = 0.00114$ kg m^2 for all the six motors.

TABLE 1. Parameters of the manipulator.

Number	Mass (kg)	Moment of inertia (kg m^2)	Centroid coordinate (m)
Link1	3.2	0.0056	$[0, 0, 0.15]^{\mathrm{T}}$
Link2	3.2	0.0044	$[0, 0, 0]^{\mathrm{T}}$
Link3	2.0	0.0035	$[0, 0, 0]^{\mathrm{T}}$
Link4	2.0	0.0031	$[0, 0, 0.1515]^{\mathrm{T}}$
Link5	1.2	0.0026	$[0, 0, 0]^{\mathrm{T}}$
Link6	1.2	0.0021	$[0, 0, -0.25]^{\mathrm{T}}$

TABLE 2. Joint friction coefficients in the simulation.

Number	f_c (Nm)	f_s (Nm)	f_v (kg m/s)	v_s (rad/s)	$f_{c\kappa}$ (Nm)
Joint1	0.49	3.5	0.15	0.19	0.05
Joint2	0.49	3.5	0.15	0.19	0.05
Joint3	0.31	2.8	0.12	0.15	0.03
Joint4	0.31	2.8	0.12	0.15	0.03
Joint5	0.1	0.7	0.03	0.03	0.01
Joint6	0.1	0.7	0.03	0.03	0.01

The desired joint trajectories for the six joints are given by [28]

$$q_n(t) = q_{dn}\left[\frac{t}{T} - \frac{1}{2\pi}\sin\left(\frac{2\pi t}{T}\right)\right], \quad 0 \le t \le T, \ 1 \le n \le 6, \tag{57}$$

where T is the simulation time. The final positions for all the joints are $q_{d1} = 90°$, $q_{d2} = 60°$, $q_{d3} = 60°$, $q_{d4} = 90°$, $q_{d5} = 60°$, $q_{d6} = 90°$, and $T = 10$ s. Fig. 7 shows the joint torques calculated by the Newton–Euler formulation and VD-based method when the desired joint trajectories, as shown in (54), are provided, and Fig. 8 shows the joint torque differences between the two methods. Table 3 contains the RMS values of these joint torque differences.

TABLE 3. RMS values of the joint torque differences.

Joint1 (Nmm)	Joint2 (Nmm)	Joint3 (Nmm)	Joint4 (Nmm)	Joint5 (Nmm)	Joint6 (Nmm)
0.2	22.7	8.9	0.6	2.3	0

As shown in Figs. 7 and 8, the simulation results with the VD-based method and Newton–Euler formulation are almost the same, with no more than 0.035 Nm differences, thus verifying the effectiveness of our proposed method. Table 3 shows that the maximum RMS values of the joint torque differences occurs at joint2, which is 22.7 Nmm, because joint2 holds the maximum load.

B. SIMULATION OF A MULTI-DOF MANIPULATOR USING VD-BASED FEEDFORWARD COMPENSATION

In this section, we utilize the VD-based dynamic model as a feedforward compensator to control the multi-DOF manipulator. A proportional-derivative controller is adopted as the

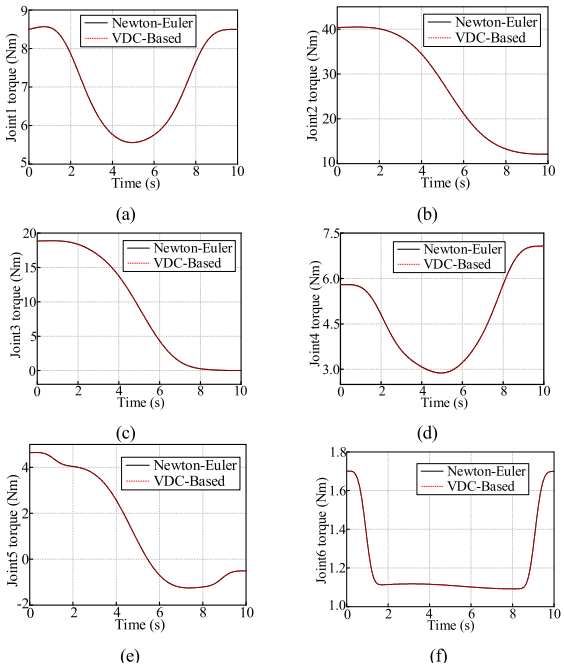

FIGURE 7. Joint torques obtained with the Newton–Euler formulation and VD-based method. (a) Joint1 torque, (b) Joint2 torque, (c) Joint3 torque, (d) Joint4 torque, (e) Joint5 torque, (f) Joint6 torque.

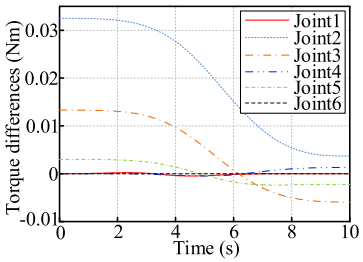

FIGURE 8. Joint torque differences.

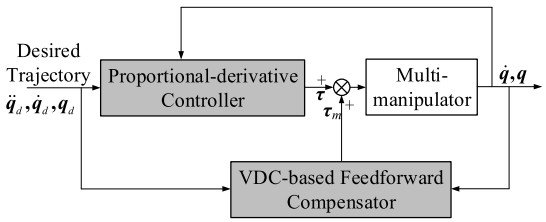

FIGURE 9. VD-based feedforward compensator for multi-DOF manipulator control.

feedback controller for the control system [29], [30], which is expressed as

$$\boldsymbol{\tau}_e = \boldsymbol{K}_v\dot{\tilde{\boldsymbol{q}}} + \boldsymbol{K}_p\tilde{\boldsymbol{q}}, \tag{58}$$

where $\boldsymbol{K}_v, \boldsymbol{K}_p \in \mathbb{R}^{6\times6}$ are the symmetric positive definite matrices chosen by the designer, and $\tilde{\boldsymbol{q}} = \boldsymbol{q}_d - \boldsymbol{q} \in \mathbb{R}^6$ denotes the position error.

Fig. 9 depicts the VD-based feedforward compensator and the proportional-derivative controller used to control the manipulator. A multi-DOF manipulator system is typically

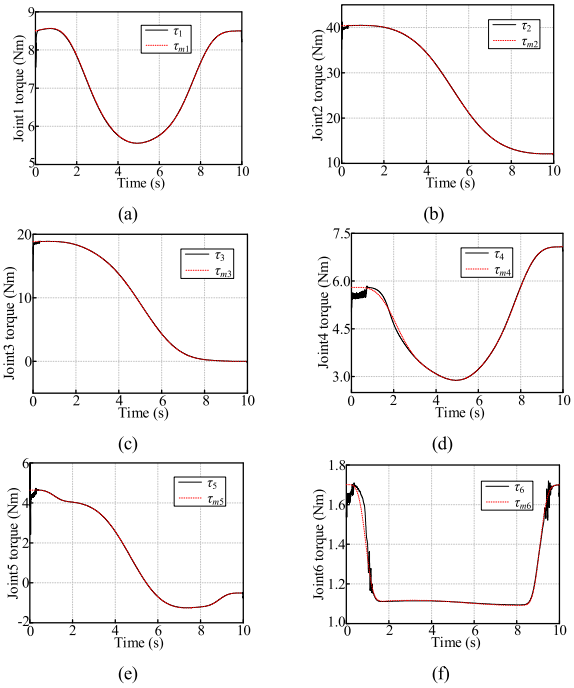

FIGURE 10. Control and feedforward torques of the manipulator. (a) Joint1 torque, (b) Joint2 torque, (c) Joint3 torque, (d) Joint4 torque, (e) Joint5 torque, (f) Joint6 torque.

TABLE 4. RMS values of the position tracking errors and torque compensation errors.

Number	RMS values of position tracking errors (°)	RMS values of torque compensation errors (Nm)
Joint1	0.0334	0.1197
Joint2	0.0115	0.4594
Joint3	0.0396	0.2381
Joint4	0.1336	0.0951
Joint5	0.0080	0.3947
Joint6	0.0470	0.0513

highly nonlinear and coupled, and the traditional Lagrangian formulation and Newton–Euler method cannot calculate the satisfactory real-time feedforward torque owing to the large computational burden. The VD-based feedforward compensator should calculate the required dynamics as closely as possible to cancel out or minimize the effect of the robot dynamics.

The desired joint trajectories in this simulation are given in (56), and are the same as those in the previous simulation. Fig. 10 shows the control torque τ and feedforward torque τ_m of the manipulator; Fig. 11 shows the joint position tracking errors and torque compensation errors of the manipulator. Table 4 contains the RMS values of the position tracking errors and torque compensation errors.

Fig. 10 shows that the compensation torque is the same as the control torque of the manipulator, implying that the proposed VD-based method can effectively calculate the robot dynamics in real time. As shown in Fig. 11(a), the joint position tracking errors are less than 0.4°, indicating that the proposed control system can effectively track the desired

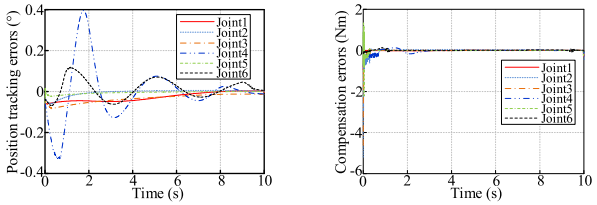

FIGURE 11. Joint position tracking errors and torque compensation errors. (a) Position tracking errors, (b) Compensation errors.

FIGURE 12. Pictures of the moving process of the manipulator. (a) shows the start position of the manipulator, (b) shows an intermediate position of the manipulator during the moving process, and (c) shows the final position of the manipulator.

trajectory. The results in Fig. 11(b) indicate that all the torque compensation errors approach zero, thus proving the accuracy of the VD-based modeling method. Table 4 shows that the maximum RMS values of the position tracking errors and torque compensation errors are no more than 0.14° and 0.5 Nm, respectively, thereby demonstrating the accuracy of the proposed modeling method in multi-DOF manipulator real-time control.

C. EXPERIMENT OF A MULTI-DOF MANIPULATOR USING VD-BASED FEEDFORWARD COMPENSATION

In this section, the proposed model has been tested as a feedforward compensator to control a real multi-DOF manipulator, the feedback controller is the same as used in Section IV.B. The test manipulator is shown in Fig. 6, and the physical parameters regarding the manipulator can be found in our previous work [23].

Only two joints have been employed in the experiment, which are joint1 and joint2, and their desired trajectories are set in the same form as (57) with $q_{d1} = 60°, q_{d2} = 30°$, and $T = 30$ s. The moving process of the manipulator is illustrated by the sequential pictures in Fig. 12.

Fig. 13 shows the desired and actual joint positions, and their position tracking errors. Fig. 14 shows the control torque τ and feedforward torque τ_m of the manipulator, and the relevant torque compensation errors. Table 5 contains the RMS values of the position tracking errors and torque compensation errors.

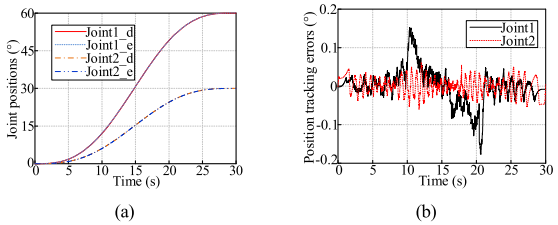

FIGURE 13. Joint positions and their tracking errors of the manipulator. (a) Joint positions, (b) Position tracking errors.

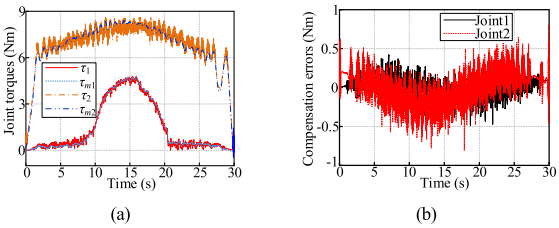

FIGURE 14. Joint torques and their compensation errors of the manipulator. (a) Joint torques, (b) Compensation errors.

TABLE 5. RMS values of the position tracking errors and torque compensation errors.

Number	RMS values of position tracking errors (°)	RMS values of torque compensation errors (Nm)
Joint1	0.0456	0.1173
Joint2	0.0227	0.2981

As shown in Fig. 13, the proposed control method can effectively track the desired joint trajectories with maximum tracking errors no more than 0.2°. Fig. 14(a) shows that, in the experiment, the compensation torques based on the proposed feedforward model can effectively estimate the robot dynamics in real time, while Fig. 14(b) indicates that there still exist some compensation errors, which are mainly caused by two factors, one is the parameter estimation errors and the other is the unmodeled dynamics. Table 5 shows that the maximum RMS values of the position tracking errors and torque compensation errors are no more than 0.05° and 0.3 Nm, respectively, thereby experimentally proving the accuracy of the proposed modeling method in real-time control of real multi-DOF manipulator.

V. CONCLUSION

A VD-based dynamic modeling method for a multi-DOF manipulator with flexible joints was developed in this study. The proposed method, the simulation results, and the experimental results were presented. The primary conclusions are summarized as follows:

(1) A deformation-related torque estimation method for a harmonic drive was applied to compute the torque caused by joint flexibility.

(2) A VD-based modeling method was presented to calculate the dynamics of a multi-DOF manipulator considering joint friction. The effect of this new method was evaluated by a contrast simulation with the Newton–Euler formulation,

and multi-DOF manipulator control simulation and experiment were conducted with a VD-based model as a feedforward compensator to verify its performance in real-time control.

(3) The contrast simulation results indicated that the accuracies of the VD-based method and Newton–Euler formulation were almost the same, with maximum differences between the RMS values of joint torques less than 30 Nmm. The control simulation and experimental results indicated the excellent performance of the proposed VD-based feedforward compensator for the real-time control, and that it could effectively estimate the dynamics of a multi-DOF manipulator with the maximum simulation RMS values of position tracking errors and torque compensation errors of less than 0.14° and 0.46 Nm, respectively, and with the maximum experimental RMS values of them less than 0.05° and 0.3 Nm, respectively.

Future work should realize robotic parameter adaptation, as the current study assumed that all the parameters were known. Additionally, this method should be improved by adding novel methods to estimate the unmodeled dynamics of the manipulator in terms of accuracy.

APPENDIX

The rigid body dynamics in $\{\mathbf{B}\}$ can be expressed as

$$ {}^{\mathbf{B}}\boldsymbol{F}^{*} = \boldsymbol{M}_{\mathbf{B}}\,{}^{\mathbf{B}}\dot{\boldsymbol{V}} + \boldsymbol{C}_{\mathbf{B}}({}^{\mathbf{B}}\boldsymbol{\omega})\,{}^{\mathbf{B}}\boldsymbol{V} + \boldsymbol{G}_{\mathbf{B}}, \tag{59} $$

with

$$ \boldsymbol{M}_{\mathbf{B}} = \begin{bmatrix} m_{\mathbf{B}}\boldsymbol{E}_3 & -m_{\mathbf{B}}({}^{\mathbf{B}}\boldsymbol{r}\times) \\ m_{\mathbf{B}}({}^{\mathbf{B}}\boldsymbol{r}\times) & \boldsymbol{I}_{\mathbf{B}} - m_{\mathbf{B}}({}^{\mathbf{B}}\boldsymbol{r}\times)^2 \end{bmatrix}, \tag{60} $$

$$ \boldsymbol{C}_{\mathbf{B}}({}^{\mathbf{B}}\boldsymbol{\omega}) = \begin{bmatrix} m_{\mathbf{B}}({}^{\mathbf{B}}\boldsymbol{\omega}\times) & -m_{\mathbf{B}}({}^{\mathbf{B}}\boldsymbol{\omega}\times)({}^{\mathbf{B}}\boldsymbol{r}\times) \\ m_{\mathbf{B}}({}^{\mathbf{B}}\boldsymbol{r}\times)({}^{\mathbf{B}}\boldsymbol{\omega}\times) & ({}^{\mathbf{B}}\boldsymbol{\omega}\times)\boldsymbol{I}_{\mathbf{B}} + \boldsymbol{I}_{\mathbf{B}}({}^{\mathbf{B}}\boldsymbol{\omega}\times) - m_{\mathbf{B}}({}^{\mathbf{B}}\boldsymbol{r}\times)({}^{\mathbf{B}}\boldsymbol{\omega}\times)({}^{\mathbf{B}}\boldsymbol{r}\times) \end{bmatrix}, \tag{61} $$

$$ \boldsymbol{G}_{\mathbf{B}} = \begin{bmatrix} m_{\mathbf{B}}\,{}^{\mathbf{B}}\boldsymbol{R}_{\mathbf{I}}\boldsymbol{g} \\ m_{\mathbf{B}}({}^{\mathbf{B}}r\times)\,{}^{\mathbf{B}}\boldsymbol{R}_{\mathbf{I}}\boldsymbol{g} \end{bmatrix}, \tag{62} $$

where $\boldsymbol{E}_3$ is a 3×3 identity matrix, $m_{\mathbf{B}}$ represents the mass of the rigid body; $\boldsymbol{I}_{\mathbf{B}}$ represents the inertia matrix of the rigid body expressed in $\{\mathbf{B}\}$; $\boldsymbol{\omega}_{\mathbf{B}}$ and $\boldsymbol{r}_{\mathbf{B}}$ represent the angular velocity and position of the center of mass of the body in $\{\mathbf{B}\}$, respectively; $\boldsymbol{g}$ represents the gravitational vector; additionally, $(\boldsymbol{q}\times)$ with a 3×1 matrix is expressed as

$$ (\boldsymbol{q}\times) = \begin{bmatrix} 0 & -q_3 & q_2 \\ q_3 & 0 & -q_1 \\ -q_2 & q_1 & 0 \end{bmatrix}, \tag{63} $$

where $\boldsymbol{q} = [q_1, q_2, q_3]^{\mathrm{T}}$.

REFERENCES

[1] S. Robla-Gómez, V. M. Becerra, J. R. Llata, E. González-Sarabia, C. Torre-Ferrero, and J. Pérez-Oria, "Working together: A review on safe human-robot collaboration in industrial environments," *IEEE Access*, vol. 5, pp. 26754–26773, 2017.

[2] S. M. Varedi, H. M. Daniali, M. Dardel, and A. Fathi, "Optimal dynamic design of a planar slider-crank mechanism with a joint clearance," *Mech. Mach. Theory*, vol. 86, pp. 191–200, Apr. 2015.

[3] W. Zheng and M. Chen, "Tracking control of manipulator based on high-order disturbance observer," *IEEE Access*, vol. 6, pp. 26753–26764, 2018.

[4] G. Buondonno and A. De Luca, "A recursive Newton–Euler algorithm for robots with elastic joints and its application to control," in *Proc. IEEE/RSJ Int. Conf. Intell. Robot. Syst.*, Hamburg, Germany, Sep./Oct. 2015, pp. 5526–5532.

[5] M. W. Spong, "Modeling and control of elastic joint robots," *J. Dyn. Syst., Meas., Control*, vol. 109, no. 4, pp. 310–318, Dec. 1987.

[6] K. Khorasani, "Nonlinear feedback control of flexible joint manipulators: A single link case study," *IEEE Trans. Autom. Control*, vol. 35, no. 10, pp. 1145–1149, Oct. 1990.

[7] M. M. Bridges and D. M. Dawson, "Redesign of robust controllers for rigid-link flexible-joint robotic manipulators actuated with harmonic drive gearing," *IEE Proc.-Control Theory Appl.*, vol. 142, no. 5, pp. 508–514, Sep. 1995.

[8] A. Ailon, M. I. Gil, E. Choi, and B.-H. Ahn, "Stabilizing robots with uncertain parameters actuated by DC motors with flexible coupling shafts," in *Proc. IEEE Int. Conf. Control Appl.*, Trieste, Italy, Sep. 1998, pp. 877–881.

[9] L. Su, Q. Hu, and L. Zhang, "Recursive decentralized control for trajectory tracking of flexible space manipulators," *IEEE Access*, vol. 7, pp. 39192–39206, 2019.

[10] H. Chaoui, P. Sicard, and A. Lakhsasi, "Reference model supervisory loop for neural network based adaptive control of a flexible joint with hard nonlinearities," in *Proc. Can. Conf. Elect. Comput. Eng.*, Niagara Falls, ON, Canada, May 2004, pp. 2029–2034.

[11] M. Ramírez-Neria, G. Ochoa-Ortega, N. Lozada-Castillo, M. A. Trujano-Cabrera, J. P. Campos-López, and A. Luviano-Juárez, "On the robust trajectory tracking task for flexible-joint robotic arm with unmodeled dynamics," *IEEE Access*, vol. 4, pp. 7816–7827, 2016.

[12] R. J. Caverly, D. E. Zlotnik, L. J. Bridgeman, and J. R. Forbes, "Saturated proportional derivative control of flexible-joint manipulators," *Robot. Comput.-Integr. Manuf.*, vol. 30, no. 6, pp. 658–666, Dec. 2014.

[13] K. Nanos and E. Papadopoulos, "On the dynamics and control of flexible joint space manipulators," *Control Eng. Pract.*, vol. 45, pp. 230–243, Dec. 2015.

[14] W.-H. Zhu, *Virtual Decomposition Control: Toward Hyper Degrees of Freedom Robots*. Berlin, Germany: Springer-Verlag, 2010.

[15] W.-H. Zhu and J. D. Schutter, "Experimental verifications of virtual-decomposition-based motion/force control," *IEEE Trans. Robot. Autom.*, vol. 18, no. 3, pp. 379–386, Jun. 2002.

[16] W.-H. Zhu and T. Lamarche, "Modular robot manipulators based on virtual decomposition control," in *Proc. IEEE Int. Conf. Robot. Autom.*, Roma, Italy, Apr. 2007, pp. 2235–2240.

[17] W.-H. Zhu, "Precision control of robots with harmonic drives," in *Proc. IEEE Int. Conf. Robot. Autom.*, Roma, Italy, Apr. 2007, pp. 3831–3836.

[18] J. Koivumäki and J. Mattila, "Stability-guaranteed impedance control of hydraulic robotic manipulators," *IEEE Trans. Mechatronics*, vol. 22, no. 2, pp. 601–612, Apr. 2017.

[19] H. Jianbin, X. Zongwu, J. Minghe, J. Zainan, and L. Hong, "Adaptive impedance-controlled manipulator based on collision detection," *Chin. J. Aeronaut.*, vol. 22, no. 1, pp. 105–112, Feb. 2009.

[20] C. T. Kiang, A. Spowage, and C. K. Yoong, "Review of control and sensor system of flexible manipulator," *J. Intell. Robot. Syst.*, vol. 77, no. 1, pp. 187–213, 2005.

[21] H. N. Rahimi and M. Nazemizadeh, " Dynamic analysis and intelligent control techniques for flexible manipulators: A review," *Adv. Robot.*, vol. 28, no. 2, pp. 63–76, 2014.

[22] T. Tjahjowidodo, F. Al-Bender, and H. Van Brussel, "Theoretical modelling and experimental identification of nonlinear torsional behaviour in harmonic drives," *Mechatronics*, vol. 23, no. 5, pp. 497–504, Aug. 2013.

[23] L. Ding, K. Xia, H. Gao, G. Liu, and Z. Deng, "Robust adaptive control of door opening by a mobile rescue manipulator based on unknown-force-related constraints estimation," *Robotica*, vol. 36, no. 1, pp. 119–140, Jan. 2018.

[24] B. Xia, G. Li, S. Yang, X. Wang, and B. Liang, "Research on virtual decomposition control of free-flying space robot with an object under nonholonomic constraints," in *Proc. IEEE Conf. Autom. Sci. Eng.*, Xi'an, China, Aug. 2017, pp. 1439–1444.

[25] L. Bascetta, G. Ferretti, and B. Scaglioni, "Closed form Newton–Euler dynamic model of flexible manipulators," *Robotica*, vol. 35, no. 5, pp. 1006–1030, May 2017.

[26] H. Zhang, S. Ahmad, and G. Liu, "Torque estimation for robotic joint with harmonic drive transmission based on position measurements," *IEEE Trans. Robot.*, vol. 31, no. 2, pp. 322–330, Apr. 2015.
[27] M. R. Kermani, R. V. Patel, and M. Moallem, "Friction identification and compensation in robotic manipulators," *IEEE Trans. Instrum. Meas.*, vol. 56, no. 6, pp. 2346–2353, Dec. 2007.
[28] A. Mohammadi, M. Tavakoli, H. J. Marquez, and F. Hashemzadeh, "Nonlinear disturbance observer design for robotic manipulators," *Control Eng. Pract.*, vol. 21, no. 3, pp. 253–267, Mar. 2013.
[29] R. Hayat, M. Leibold, and M. Buss, "Robust-adaptive controller design for robot manipulators using the $\mathcal{H}_\infty$ approach," *IEEE Access*, vol. 6, pp. 51626–51639, 2018.
[30] M. W. Spong, S. Hutchinson, and M. Vidyasagar, *Robot Modeling and Control*. New York, NY, USA: Wiley, 2005.

KERUI XIA was born in 1987. He received the M.Sc. and Ph.D. degrees from the Harbin Institute of Technology, in 2012 and 2017, respectively. He is currently the Leader of the Drive and Control Group, Industrial Intelligent Equipment Institute, HRG International Institute for Research & Innovation, China. His research interests include robot system control, intelligent control, and mobile manipulation.

HONGJUN XING was born in 1992. He received the B.Sc. and M.Sc. degrees from the Harbin Institute of Technology, China, in 2015 and 2017, respectively, where he is currently pursuing the Ph.D. degree with the School of Mechatronics Engineering. His research interests include dynamic modeling, tele-robotics, and compliance control.

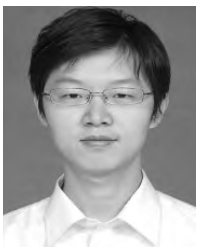

LIANG DING (M'10–SM'18) was born in 1980. He received the Ph.D. degree in mechanical engineering from the Harbin Institute of Technology, China, in 2010, where he is currently a Professor and a Ph.D. candidate supervisor. His research interests include mechanics, and the control and simulation of mobile robots.

HAIBO GAO was born in 1970. He received the Ph.D. degree in mechanical engineering from the Harbin Institute of Technology, China, in 2003, where he is currently a Professor and a Ph.D. candidate supervisor. His research interest includes aerospace mechanism and control.

GUANGJUN LIU (M'99–SM'08) received the B.E. degree from the University of Science and Technology of China, Hefei, China, in 1984, the M.E. degree from the Chinese Academy of Sciences, Shenyang Institute of Automation, Shenyang, China, in 1987, and the Ph.D. degree from the University of Toronto, Toronto, ON, Canada, in 1996. He is currently a Professor and the Canada Research Chair in control systems and robotics with the Department of Aerospace Engineering, Ryerson University, Toronto. His research interests include control systems and robotics, particularly in modular and reconfigurable robots, mobile manipulators, and aircraft systems.

ZONGQUAN DENG was born in 1956. He is currently a Professor and a Ph.D. candidate supervisor with the Harbin Institute of Technology, China. His research interests include special robotics, and aerospace mechanism and control.